American Journal of Electrical and Electronic Engineering, 2016, Vol. 4, No. 4, 110-122
Available online at http://pubs.sciepub.com/ajeee/4/4/2
©Science and Education Publishing
DOI:10.12691/ajeee-4-4-2

A Study on Overvoltage Distribution Across the High Voltage Winding of an Electric Power Transformer

Gloria Ciumbulea[1], Lavinia Iordache (Bobaru)[1], Sorin Deleanu[2,*], Mihai Iordache[1], Neculai Galan[1], Scott Basinger[3], Gregory Von Lipinski[2], David Carpenter[4]

[1]"POLITEHNICA" University of Bucharest, Bucharest, Romania
[2]Northern Alberta Institute of Technology, Edmonton, Canada
[3]Eaton Corporation, Edmonton, Canada
[4]GE's Grid Software Solutions, Technical Training Institute, Redmond, Washington, USA
*Corresponding author: sorind@nait.ca, sorin1365@gmail.com

Abstract The main objective of this paper is to represent effects of overvoltage on a transformer winding by analysis and modelling with special attention given to the voltage distribution across the winding. The authors have considered both approaches in modelling the winding: windings with distributed electrical parameters, and secondly disk coils with concentrated parameters. All known models are assembled in a general model based upon distributed parameters, while the excitation voltages display sinusoidal variation in time (commutation) or step. Both induced and commutation voltages, applied across the transformer winding, will generate free oscillations which are analyzed further on. According to the model, the transformer's windings are divided in several disk coils with concentrated known parameters. This results in a complete electrical network used for simulations. All simulations have been performed using the software package SYSEG (SYmbolic State Equation Generation). Using SYSEG package, from the state equations assembled in terms of the disk coils voltages, one can obtain the overvoltage across the transformer winding as function of time. If the frequency of the commutation voltage and the frequency of the free oscillations are in close range, then the voltage across the disk coils shows a non-uniform distribution. An important aspect of this paper is accounting for asymmetry of the transformer by modelling the reinforced insulation of the first turns of the disk coils of the transformer's high voltage winding. This affects the value of the inter-turn capacitance of these coils, and is an aspect which is treated in our simulations.

Keywords: *transformer, overvoltage, modeling, disk coils, simulation, resonance*

Cite This Article: Gloria Ciumbulea, Lavinia Iordache (Bobaru), Sorin Deleanu, Mihai Iordache, Neculai Galan, Scott Basinger, Gregory Von Lipinski, and David Carpenter, "A Study on Overvoltage Distribution Across the High Voltage Winding of an Electric Power Transformer." *American Journal of Electrical and Electronic Engineering*, vol. 4, no. 4 (2016): 110-122. doi: 10.12691/ajeee-4-4-2.

1. Introduction

When considering the time variation one can classify overvoltages as fast transient (FTO), and, very fast transient (VFTO). The overvoltages across the transformer windings can be triggered by external causes such as atmospheric electrical discharges in the neighborhood of the installations containing the transformers or even onto it. They can also be triggered by internal causes such as commutation following connection/disconnection procedures in the installations containing lines and transformers, fast transient phenomena such as current chop from circuit interrupters, overcurrent situations, etc.

Specific aspects regarding the occurrence of overvoltages across transformer windings have been studied over time and many publications are available [1-24].

Two types of overvoltages are taken into consideration: aperiodic pulses of short duration, respectively periodic waveforms. Both have magnitudes which can significantly exceed the rated voltage value of the transformer. When operating the commutation equipment, the overvoltages last less than 0.1 μs, while the oscillation component displays a frequency of several MHz with durations in range of microseconds. The oscillations of the overvoltage waveforms are dangerous due to the resonance phenomenon, usually recorded for fast transients. This is caused by the capacitances and inductances of the overall transformer winding. Due to the fact that for high frequencies the magnetic field doesn't penetrate the ferromagnetic core of the transformer, the only magnetic field taken into consideration is the leakage one produced by the high voltage winding. Despite the fact that the turns are series connected, the current through the entire winding doesn't have the same value. This fact is explained by the presence of the inherent local capacitors formed between the winding and the ground, respectively between the high voltage windings and the adjacent windings. Consequently, the space distribution of the magnetic field becomes more complicated.

The precision of parameter determination at high frequency is of great importance when accurate overvoltage distribution is required.

There are many literature resources focused on the determination winding parameters, mostly presenting numerical methods based upon either Finite Element Analysis (FEA) or Bounday Element Method (BEM) analytical calculation.

Numerical 2D and 3D FEA applied to evalute the winding capacitance [7] is completed by analytical calculations [21,22,23], while the value of the capacitance obtained with 3D BEM is compared to those obtained using 2D FEM in [12]. In [8] and [11] mutual inductance between two coils of the winding is evaluated numerically and analytically as well, while the complete calculation of inductance matrix for the transformer windings is described in [15].

In [12] and [13], the authors use the 3D Modelling of the power transformer for determination of the effective parmeters of the windings, inductance and reistance. In references [16,17], transformer reactance is obtained through detailed calculations based upon the analytical integration of the vector potential *A*.The mathematical model developed for the winding with distributed parameters has two parts:

Part I: the model of the single phase long lines

Part II: the model used to determine the distribution of the overvoltage across the winding

The final form of the model is represented by the voltage equation, described in terms of partial derivatives.

When solving the equation for known parameters, one ca assess the overvoltage across the transformer winding in the following steps [25,26]:

a. Apply the "RLC Ladder Netwok" which consists of dividing the high voltage winding into disk coils model for the purpose of calculating the overvoltage distribution across the winding
b. Run SYSEG program to obtain the maximum initial values of the voltages across the individual disk coils

Once calculated, the values of the voltages across each of the disc coils give useful information regarding the procedure used to design/configure the insulation for the winding.

Simulations performed with the application of very high frequency alternating voltages, emulating the commutation voltages, respectively step voltages, delivered important results.

If the commutation voltage has a pulsation in the range of the resonance frequency of free oscillations, then the distribution of the overvoltage is least favourable, revealing large amount of voltage drop only across some disc coils. The amount of dielectric stress of the insulation of those coils is significant. If the pulsation of the commutation voltage decreases, the overvoltage distribution becomes more uniform, without completely eliminating the voltage levels that can be dangerous for the insulation.

2. Modelling the High Voltage Winding of the Transformer for Overvoltages Study Purpose

Most of the studies consider two categories of models regarding the high voltage winding overvoltage stress analysis:

a) The model built with the consideration of the line with distributed parameters (similar to the long electrical lines theory)

b) The model based upon concentrated parameters

Each of the models has two versions due to the fact that the neutral point of the winding (wye-connected) is either isolated or connected to the ground. In terms of the occurrence of physical phenomena in the windings, the application the two models brings significantly different results when analyzing the distribution and propagation of the overvoltage waveform across the winding. In the same time, the two models treat differently the phenomenon of the overvoltage waveform reflection at the borders between the winding zones which are characterized by different values for parameters.

2.1. Modelling the System with Distributed Parameters

For the three-phase transformer with distributed parameters, the values of the capacitance and conductivity between one phase high voltage winding (AX) and the other two (BY, CZ) are considered negligible. The proposed equivalent circuit for the model with distributed parameters is presented in Figure 1.

The notations for the specific parameters per unit of length used further are *R*, R_i , *L*, *K*, *C* and *G*. *R[Ω/m]* represents the resistance of the transformer winding per unit of length, R_i *[Ω/m]* represents the resistance of the insulation of the winding conductor per unit of length, *L[H/m]* represents the inductivity of the transformer winding per unit of length, *K[F/m]* represents the capacitance of the transformer winding per unit of length, *C[F/m]* represents the capacitance of the transformer winding per unit of length with respect to the ground, *G[S/m]* represents the conductance of the transformer winding per unit of length.When applying the Kirchhoff's Current Law (KCL) in the nodes *a, a'*, followed by the Kirchhoff's Voltage Law (KVL) across the closed circuit loop *aa'bb'*, one can obtain the system of equations (1)-(13).

In (1)-(13) the symbols *u* and *i* represent the voltage, respectively the current at the distance *x* from the input terminal A (in conformity with the theory of the long electric lines).

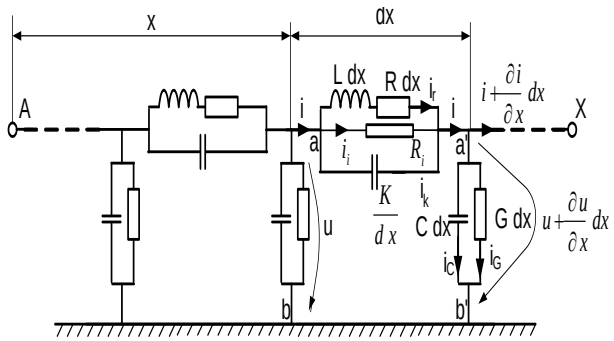

Figure 1. The equivalent circuit for the model with distributed parameters

$$i = i_r + i_k + i_i \tag{1}$$

$$i - \left(i + \frac{\partial i}{\partial x} dx \right) - \left(C \frac{\partial u}{\partial t} + G u \right) dx = 0 \tag{2}$$

$$\frac{dx}{K}\int i_k dt + \left(u + \frac{\partial u}{\partial x} dx\right) - u = 0 \tag{3}$$

$$\frac{dx}{K}\int i_k dt = \left(R i_r + L\frac{\partial i}{\partial t}\right) dx = R_i i_i \, dx \tag{4}$$

$$-\frac{\partial i}{\partial x} = C\frac{\partial u}{\partial t} + G \tag{5}$$

$$\frac{i_k}{K} = R\frac{\partial i_r}{\partial t} + L\frac{\partial^2 i_r}{\partial t^2} = R_i\frac{\partial i_i}{\partial t} = -\frac{\partial^2 u}{\partial x \partial t} \tag{6}$$

$$i_k = -K\frac{\partial^2 u}{\partial x \partial t} \tag{7}$$

$$i_i = -G_i\frac{\partial u}{\partial x} \tag{8}$$

$$G_i = \frac{1}{R_i} \tag{9}$$

$$i_r = i + K\frac{\partial^2 u}{\partial x \partial t} + G_i\frac{\partial u}{\partial x} \tag{10}$$

$$R\left(\frac{\partial i}{\partial t} + K\frac{\partial^3 u}{\partial x \partial t^2} + G_i\frac{\partial^2 u}{\partial x \partial t}\right) = f(x,t) \tag{11}$$

$$L\left(\frac{\partial^2 i}{\partial t^2} + K\frac{\partial^4 u}{\partial x \partial t^3} + G_i\frac{\partial^3 u}{\partial x \partial t^2}\right) = g(x,t) \tag{12}$$

$$f(x,t) + g(x,t) = -\frac{\partial^2 u}{\partial x \partial t}. \tag{13}$$

In the system (1)-(13), when deriving with respect to the variable x and substituting for the current i, one can obtain a differential equation with partial derivatives (14)-(17) in terms of the voltage u.

$$LK\frac{\partial^5 u}{\partial x^2 \partial t^3} + (RK + LG_i)\frac{\partial^4 u}{\partial x^2 \partial t^2} = h(x,t) \tag{14}$$

$$RG_i\frac{\partial^3 u}{\partial x^2 \partial t} - LC\frac{\partial^3 u}{\partial t^3} = m(x,t) \tag{15}$$

$$(RC + LG)\frac{\partial^2 u}{\partial t^2} + RG\frac{\partial u}{\partial t} = n(x,t) \tag{16}$$

$$h(x,t) + m(x,t) - n(x,t) = -\frac{\partial^3 u}{\partial x^2 \partial t} \tag{17}$$

The equations (14)-(17) represent an extension of the already known equations of the systems with distributed parameters. When imposing $K = 0$ and $R_i = 0$, the equations (14)-(17) are reunited under the classical voltage equation of the long lines, while for $G_i = 0$, the same equations (2) are used to solve and study the overvoltage distribution across the winding of the transformer. The occurrence of dielectric loss, which cannot be neglected at high frequencies, motivates the presence of G and G_i in the model of the insulation. The differential equation with partial derivatives of the voltage u has an increased order when introducing the capacitances C and K. The solution of the voltage equation, which describes the voltage u as "time" and "space" function, is much different in the new conditions.

For simplification reasons, we've considered the conductivity along the insulation of an element $G_i = 0$. This statement is justified by the fact that it is highly unlikely for the leakage current to circulate along the insulation of the high voltage winding under study.

When applying the Laplace Transform for equations (14)-(17), the voltage equation is reshaped in (18):

$$\begin{aligned} &KLp^2\frac{\partial^2 u(p)}{\partial x^2} + KRp\frac{\partial^2 u(p)}{\partial x^2} + \frac{\partial^2 u(p)}{\partial x^2} + \ldots \\ &-LCp^2 u(p) - (RC + LG)pu(p). - RGu(p) = 0 \end{aligned} \tag{18}$$

With adequate initial conditions (null) will obtain (19):

$$\frac{\partial^2 u(p)}{\partial x^2} - \lambda^2 u(p) = 0. \tag{19}$$

The coefficient λ^2 is given by (20).

$$\lambda^2 = \frac{LCp^2 + (RC + LG)p + RG}{KLp^2 + KRp + 1}. \tag{20}$$

A generic solution of the equation (20) is given in (21) or (22).

$$u(p) = A e^{\lambda x} + B e^{-\lambda x} x \tag{21}$$

$$u(p) = A' ch\lambda x + B' sh\lambda \tag{22}$$

The values of the constants A and B, respectively A' and B' are uniquely determined for boundary conditions ($x = 0$ and $x = l$), where l is the length of the winding.

Equations (14)-(17) for $G_i \neq 0$ can be presented simpler, clearer and easier to use as (23).

$$\begin{aligned} &\frac{\partial^4 u}{\partial x^2 \partial t^2} + \frac{R}{L}\frac{\partial^3 u}{\partial x^2 \partial t} + \frac{1}{KL}\frac{\partial^2 u}{\partial x^2} - \frac{C}{K}\frac{\partial^2 u}{\partial t^2} + \ldots \\ &\ldots + \left(\frac{RC}{KL} + \frac{GC}{KC}\right)\frac{\partial u}{\partial t} - \frac{RG}{KL}u = 0 \end{aligned} \tag{23}$$

$$\begin{aligned} &\frac{\partial^4 u}{\partial x^2 \partial t^2} + \rho\frac{\partial^3 u}{\partial x^2 \partial t} + \beta\frac{\partial^2 u}{\partial x^2} - \alpha^2\frac{\partial^2 u}{\partial t^2} + \ldots \\ &\ldots - \alpha^2(\rho + \gamma)\frac{\partial u}{\partial t} - \rho\alpha^2\gamma u = 0 \end{aligned} \tag{24}$$

$$\alpha^2 = \frac{C}{K} \tag{25}$$

$$\rho = \frac{R}{L} \tag{26}$$

$$\beta = \frac{1}{KL} \tag{27}$$

$$\gamma = \frac{G}{C} = \frac{G}{\alpha^2 K} \tag{28}$$

$$G_i = 0. \tag{29}$$

The identities (25)-(29) facilitate the simplification of the voltage equation from above. In order to obtain the solutions of equations (21)-(22) in the time domain, one can choose certain specialized software package(s), upon availability. However, the existing numerical methods have the capability of direct integration for the equations (14)-(17) and/or (23)-(24).The authors highlight another procedure for obtaining the solution of the equation with partial derivatives for (14)-(17) when $G_i = 0$. This is the well-known method of separating the variables, in which is assumed a solution of the following type:

$$u(x,t) = X(x)\cdot T(t). \tag{30}$$

When substituting (30) in the equation with partial derivatives (23), will result the following relationships:

$$\begin{aligned} &X''(x)\cdot T''(t)+\rho X''(x)\cdot T'(t)+\beta X''(x)\cdot T(t) \\ &-\alpha^2 X(x)\cdot T''(t)-\ldots-\alpha^2(\rho+\gamma)X(x)\cdot T'(t) \\ &-\rho\,\alpha^2 X(x)\cdot T(t)=0 \end{aligned} \tag{31}$$

$$\begin{aligned} &X''(x)\cdot\left[\,T''(t)+\rho T'(t)+\beta T(t)\,\right]-\ldots \\ &\ldots-X(x)\cdot\begin{bmatrix}\alpha^2 T''(t)+\alpha^2(\rho+\gamma)T'(t) \\ +\rho\,\alpha^2 T(t)\end{bmatrix}=0 \end{aligned} \tag{32}$$

$$\frac{X''(x)}{X(x)}=\frac{\alpha^2 T''(t)+\alpha^2(\rho+\gamma)T'(t)+\rho\,\alpha^2 T(t)}{T''(t)+\rho T'(t)+\beta T(t)} \tag{33}$$

$$= const.$$

The equation with partial derivatives is equivalent to two differential equations of second order with constant coefficients. These equations can be solved separately.

The equation with the independent variable x requires border conditions, while the one with independent variable t requires initial conditions.

2.2. Modelling the System with Concentrated Parameters

For this model, the transformer winding with overvoltage across is composed by a series of connected disk coils. The final result is an electrical network built up with discrete elements of concentrated parameters.

There are two categories of calculation models treated in the literature: Gray Box Model and Black Box Model.

Gray Box Model is typically used for design purposes, when studying the transformer winding under the resonance conditions, highlighting the voltage distribution across the winding. This model consists of a combination of RLC Ladder Network and Multi-conductor Transmission Line Model – MTL [1,2,3,4].

The RLC Ladder Network is a model in which R, L, C are concentrated parameters. Initial version of the model (based upon "flat coils") had limited frequency range in terms of kilohertz while the present version (based upon "turn-by-turn") can offer modeling capabilities in the range of megahertz.The RLC Ladder Model is the best choice when involving the transient study under overvoltage conditions. The main reason is represented by the possibilities of assembling very accurate and complex equivalent circuits of the transformer windings. However, for high voltage transformers with high power ratings, , the model of transformer winding using "turn-by-turn" basis can become cumbersome and present difficulties to simulate. When modelling the transformer winding, the disk coil has an equivalent circuit with multiple structure and parameters displayed in Figure 2 [2,3].

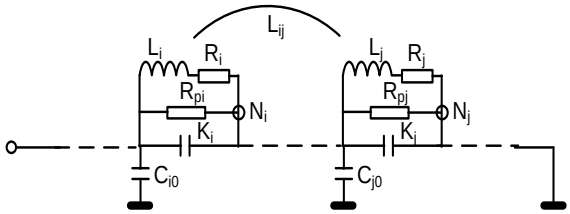

Figure 2. The Disk Coils *I* and *j* from the RLC network [2]

The base element of the model is composed by the disk coil with all of the three branches connected in parallel with the capacitance C_{i0} with respect to the ground (according to Figure 2).

Series connected elements R_i and L_i represent the resistance, respectively the inductance of the disk coil, while K_i is the equivalent capacitance between the coil's turns. The capacitor K_i has dielectric losses symbolized here by the resistance R_{pi}. The only mutual inductivities L_{ij} accounted for in the model are those between two coils (*i* and *j* for example), while the mutual inductivities between the turns belonging to the same coil are neglected. The entire model suffers very benefic simplifications in in this way.

When applying Kirchhoff's equations one can obtain the equations for currents, voltages and operational impedances referring the *N* nodes, assembled in a matrix form.

Similar models are currently used for the study of the over-voltage at the terminals of rotational motors [5,6].

2.3. Electrical Parameters Used in Modelling and Studying the Overvoltage Phenomena

The accurate knowledge of the electrical parameters like resistance, conductivity, inductance and capacitance, was proven essential when modelling the transformer with the purpose of studying the overvoltages. There are many published papers, focused on the topic of the transformer's windings stress due to overvoltage [7-23], and they represent clear and significant contributions. Further, this section is dedicated to important elements concerning the electrical parameters.

In every modelling procedure, resistance, as parameter, must be evaluated including the complete skin effect which is occurring at high frequencies and for fast transients of the current through conductor.

The capacity per of length, as element of a matrix, can be calculated applying FEM. It is assumed that there are *N* conductors; the conductor *j* has 1*volt* across, and the other conductors are connrcted at a potential equal to zero [24].

The relations used for the purpose of calculating the capacitances are:

$$C_{ij}=\frac{q_i}{\Delta U_{ij}},\, i\neq j\,;\, W_j=\frac{1}{2}\sum_{i=1}^{N} C_{ij}\Delta U_{ij}^2 \tag{34}$$

where: C_{ij} - capacitance between the conductor i and the conductor j; q_i – the electrical charge of the conductor i; ΔU_{ij} –potential difference between the conductor i and the conductor j; W_j – the energy of the electrostatic field of the system. W_j can be easily calculated with an adeaquate FEM software package (Ansys, Opera, etc.) This method can be exemplified using the rectangular conductor system given in Figure 3.a. Voltage is applied to conductor 5 and the energy of the electrostatic field W_5 is calculated; similarly for conductor 4, the energy W_4 and for conductor 8 we obtain W_8. Given this, there are the following equations available (35):

$$\begin{aligned}
&\frac{1}{2}C_s\Delta U_{52}^2+\frac{1}{2}C_s\Delta U_{58}^2+\frac{1}{2}C_k\Delta U_{54}^2+\frac{1}{2}C_k\Delta U_{56}^2=W_5;\\
&\Delta U_{52}=\Delta U_{58}=\Delta U_{54}=\Delta U_{56}=1V;\\
&\frac{1}{2}C_s\Delta U_{41}^2+\frac{1}{2}C_s\Delta U_{47}^2+\frac{1}{2}C_k\Delta U_{45}^2+\frac{1}{2}C_g\Delta U_{40}^2=W_4;\\
&\Delta U_{41}=\Delta U_{47}=\Delta U_{45}=\Delta U_{40}=1V;\\
&\frac{1}{2}C_s\Delta U_{85}^2+\frac{1}{2}C_k\Delta U_{87}^2+\frac{1}{2}C_g\Delta U_{89}^2=W_8;\\
&\Delta U_{85}=\Delta U_{87}=\Delta U_{89}=1V.
\end{aligned} \tag{35}$$

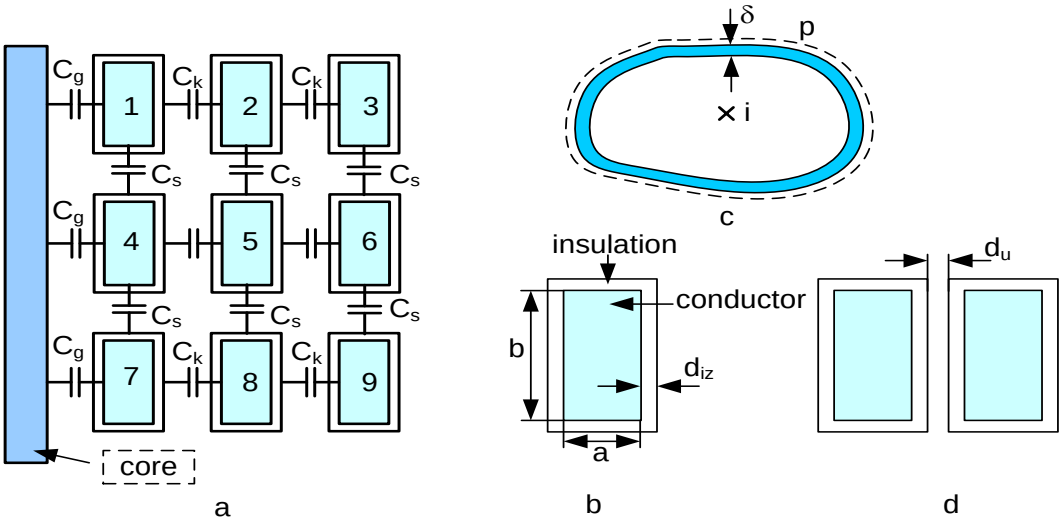

Figure 3. **a)** Arrangement of the conductors of a part from the transformer winding; **b)** details with regard to the conductor; **c)** conductor with a given section crossed by the current i; **d)** the positioning of two conductors for the calculation of capacity. a and b are the sizes of the rectangular conductor, d_{iz} – thickness of the conductor insulation, d_u – thickness of the oil layer between conductors, p – conductor perimeter, δ - thickness of the penetration depth for a net Kelvin effect

Based on the equations (35), the capacitances are related to the electrostatic energies through the matrix equations (36). In this way capacitances C_s, C_k and C_g are calculated, once knowing the electrostatic energy.

$$\begin{bmatrix} 1 & 1 & 0 \\ 1 & 0,5 & 0,5 \\ 0,5 & 1 & 0 \end{bmatrix}\begin{bmatrix} C_s \\ C_k \\ C_g \end{bmatrix}=\begin{bmatrix} W_5 \\ W_4 \\ W_8 \end{bmatrix}. \tag{36}$$

Using this calculation method, the capacitances between the turns, repectively between the turns and the ground are determined with a better accuracy due to the inclusion of the “end effect”, otherwise neglected. The capacity between two conductors can be calculated with simple relations if the end effect is neglected also (the electric field is uniform between the two conductors). For example we consider the conductors from Figure 3.d. Knowing that the normal component D_n of the electrical induction is preserved at the separation surface of two media, then the necessary relations to determine the capacity between the two conductors are (37), (38):

$$\begin{aligned}
&D_{niz}=\varepsilon_{iz}E_{niz}=\varepsilon_u E_{nu}=\frac{q}{A};\quad A=b\cdot l;\\
&U=2d_{iz}E_{niz}+d_u E_{nu}\Rightarrow C=\frac{q}{U}=\frac{A}{\dfrac{2d_{iz}}{\varepsilon_{iz}}+\dfrac{d_u}{\varepsilon_u}}
\end{aligned} \tag{37}$$

$$C=\frac{A}{\sum_{i=1}^{n}\dfrac{d_i}{\varepsilon_i}} \tag{38}$$

where D_n and E_n are the normal components of the electrical induction and respectively the intensity of the electric field; l is the conductor's length; q is the electric charge; U is the voltage between the faces of the two conductors. In relation (37), it was also given the general expression of a plain capacitor where the insulation between plates is made of n plain layers with different dielectric constants ε_i.

The resistance per unit of length should be calculated considering the net Kelvin effect taking place at high frequencies or for fast current variations through the conductor.

On net Kelvin effect, the current i is distributed close to the conductor surface with the penetration depth δ (Figure 7.c); for a given surface of the conductor section, resistance R_δ is calculated, while for the rectangular surface, the resistance R_{dr} is calculated.

$$\begin{aligned}
&R_\delta=\frac{1\cdot\rho}{p\,\delta};\ \delta=\sqrt{\frac{2\rho}{\omega\mu}}=\sqrt{\frac{1}{\pi\sigma f\mu}}\Rightarrow R_\delta=\frac{1}{p}\sqrt{\frac{\pi f\mu}{\sigma}};\\
&R_{dr}=\frac{1}{2(a+b)}\sqrt{\frac{\pi f\mu}{\sigma}};\quad \rho=\frac{1}{\sigma}
\end{aligned} \tag{39}$$

ρ and μ are the electrical resistivity, respectively magnetic permeability of the conductor material; for copper $\mu = \mu_0$.

The inductance per unit of length L_l is more difficult to calculate. This inductance has two components: one component, L_e, due to the magnetic field from outside the conductor, and the other component L_i, due to the magnetic field from inside the conductor.

To calculate the component L_e it is necessary to use the propagation speed of the electromagnetic filed v_0.

The overvoltage waves propagate through the dielectric media where $\mu = \mu_0$ and $\varepsilon = \varepsilon_0\ \varepsilon_r$, ε_r being the relative dielectric permittivity of the propagation medium, expressed in p.u. In this case, only the capacitance is subjected to change depending on the dielectric characteristics. The following relations become available:

$$\begin{aligned} v_0 &= \frac{1}{\sqrt{L_l C_l}} = \frac{1}{\sqrt{L_l C_{l0} \varepsilon_r}} = \frac{c}{\sqrt{\varepsilon_r}} \\ L_l &= \frac{\varepsilon_r}{c^2 C_l} = L_e \\ C_l &= \frac{A\varepsilon}{d} = \frac{A\varepsilon_0 \varepsilon_r}{d} = C_{l0}\varepsilon_r; \\ C_{l0} &= \frac{A\varepsilon_0}{d}; c = \frac{1}{\sqrt{L_l C_{l0}}} \end{aligned} \tag{40}$$

where c is the speed of light determined by the constants μ_0 and ε_0; C is proportional with the electric constant $\varepsilon = \varepsilon_0\ \varepsilon_r$ and then we can write the relation $C = C_0\ \varepsilon_r$ where C_0 is determined by ε_0. The capacity C_l can be relatively easy determined from the relation (40), resulting the inductance L_e.

To calculate the component L_i we've considered the case of the electromagnetic field penetration in the cconducting semi-infinite space.

When the skin effect occurs, the current is distributed towards the outside surface of the conductor, with a depth of penetration δ.

For a cylindrical conductor, with the cross sectional area S, the Kelvin effect is valid if the condition $\delta << S^{1/2}$ is fulfilled.

For valid Kelvin effect, the expression of the wave impedance $\underline{Z}$ has the real part R equal with the imaginary part ωL, obtaining:

$$\begin{aligned} \underline{Z} &= \frac{\underline{E}}{\underline{H}} = R + j\omega L; \quad R = \omega L \\ R &= R_S;\ L = L_i \Rightarrow L_i = \frac{R_S}{\omega} = \frac{R_S}{2\pi f} \end{aligned} \tag{41}$$

i.e. that when the pulsation ω is known, the inductance L_i is calculated from the previously determined resistance R_s, The total leakage inductance L_l is: $L_l = L_e + L_i$.

For a more precise calculation, [8] recommends the physical model from Figure 4, where the core with radius a is has an infinite length. This assumption is justified by the Krarup model for the magnetic core of the transformer, which forms a closed loop, and the end effects can be neglected.

The magnetic core, being made from cold-laminated, silicon alloy, iron metal sheets displays magnetia anisotropy and therefore the p.u. magnetic permeability μ_r after direction $0r$ and p.u. magnetic permeability μ_z after direction $0z$ have different values.

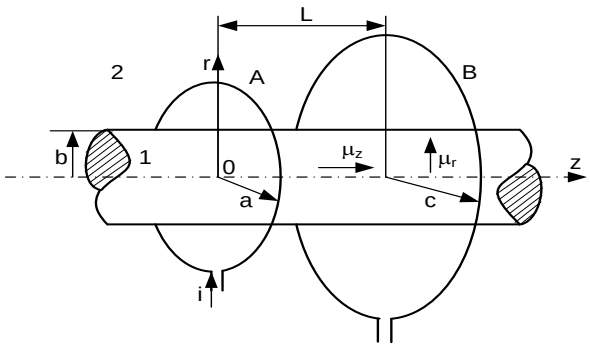

Figure 4. Filamentary turns arranged concentrically on the Krarup core

The conductivity of medium *1* is σ. Other data are given in Figure 4. At this point, for the purpose of calculating the self and mutual inductances, it is necessary to establish the vector potential equation. The vector potential directly relates to the magnetic field produced by the current i.

For this magnetic field with axial symmetry, the magnetic vector potential, in cylindrical coordinates (r, α, z), has only one component different from zero, i.e. the component $A\alpha$, fact that leads to simpler calculations.

Due to the fact that the magnetic field has axial symmetry, the component $A\alpha$ depends only on the coordinates r and z, i.e. $A\alpha(r,z)$. We start from the following vector equations:

$$\vec{B} = rot\,\vec{A};\ div\,\vec{A} = 0;\ rot\,\vec{H} = \vec{J}. \tag{42}$$

Because the Krarup core is magnetically anisotropic with μ_r p.u. magnetic permeability along the direction r, and μ_z p.u. magnetic permeability in the direction z, the equation refers only to the term $A\alpha$.

Asssuming sinusoidal variation in time, the equation of component $\underline{A}\alpha_1$ in area 1 ($r \le b$) is:

$$\begin{aligned} &\frac{1}{r}\frac{\partial}{\partial r}\left(r\frac{\partial \underline{A}_{\alpha 1}}{\partial r}\right) + \frac{1}{a^2}\frac{\partial^2 \underline{A}_{\alpha 1}}{\partial z^2} = j\omega\mu_z\sigma\underline{A}_{\alpha 1\alpha}; \\ &a = \sqrt{\frac{\mu_r}{\mu_z}}; \quad \gamma^2 = j\omega\mu_z\sigma; \end{aligned} \tag{43}$$

For area 2 (r ≥ b), the magnetic potential $A\alpha_2$ can be separated in two terms:

$$\begin{aligned} &\underline{A}_{\alpha 2} = \underline{A}'_{\alpha 2} + \underline{A}''_{\alpha 2} \\ &r \ge b; \quad \frac{1}{r}\frac{\partial}{\partial r}\left(r\frac{\partial \underline{A}'_{\alpha 2}}{\partial r}\right) + \frac{1}{a^2}\frac{\partial^2 \underline{A}'_{\alpha 2}}{\partial z^2} = 0; \\ &r \le a; \quad A_{\alpha 2} = \frac{\underline{I}\,\mu_0}{\pi}\int_0^\infty K_1(\lambda a) I_1(\lambda r)\cos\lambda z\, d\lambda \end{aligned} \tag{44}$$

where I_1(x) and K_1(x) are the modified Bessel functions of *1st* and *2nd* order.

Applying the method of the separation of variables the component $\underline{A}\alpha_i$ (i = 1; 2) can be put under the form:

$$A_{\alpha i} = A_{\alpha i}(r, z) = R_i(r)\,Z_i(z) = R_i\ Z_i;\ i = 1; 2. \tag{45}$$

The component A_{zi} is given for the two separate magnetic fields *1* and *2* as the product of two functions *R(r)* and *Z(z)* according to the method of the separation of variables, resulting two differential equations are obtained (46)

$$\frac{1}{R_i}\left(\frac{d^2R_i}{dr^2}+\frac{1}{r}\frac{dR_i}{dr}\right)-\gamma^2=-\frac{1}{a^2}\frac{1}{Z_i}\frac{d^2Z_i}{dz^2}=\lambda^2$$

$$\begin{cases}\dfrac{d^2R_i}{dr^2}+\dfrac{1}{r}\dfrac{dR_i}{dr}-\left(\gamma^2+\lambda^2\right)R_i=0\\ \dfrac{d^2Z_i}{dz^2}+\lambda^2a^2Z_i=0\end{cases} \tag{46}$$

The first differential equation from (46) is a Bessel equation which was made equivalent with the next two equations. The solutions of the two differential equations are (47):

$$zone\,1$$

$$\begin{cases}R_1(r)=P_{\lambda1}I_1\left(r\sqrt{\gamma^2+\lambda^2}\right)+R_{\lambda1}K_1\left(r\sqrt{\gamma^2+\lambda^2}\right);\\ Z_1(z)=S_{\lambda1}\cos(\lambda az)+T_{\lambda1}\sin(\lambda az)\end{cases}$$

$$zone\,2,\ \gamma=0; \tag{47}$$

$$\begin{cases}R_2(r)=P_{\lambda2}I_1(r\lambda)+R_{\lambda2}K_1(r\lambda);\\ Z_2(z)=S_{\lambda2}\cos(\lambda z)+T_{\lambda2}\sin(\lambda z)\end{cases}$$

$$\Rightarrow A'_{\alpha2}=R_2(r)Z_2(z)$$

In order to determine the constants resulting from the integration, suitable border *(r = b)* conditions are necessary: The conditions of surface crossing are inserted, *r = b*, to determine the integration constants; there are two conditions:

1. The preservation of the magnetic field intensity components which are tangent to the border; additionally the current at the surface of separation between the two media, with the density J_s, can be extracted from the axial component A_α of the magnetic vector potential, calculated for the two adjacent areas:

$$H_{i1}-H_{i2}=H_{z1}-H_{z2}=J_s$$
$$\Leftrightarrow\frac{1}{\mu_z}\frac{\partial A_{\alpha1}}{\partial r}\Big|_{r=b}-\frac{1}{\mu_0}\frac{\partial A_{\alpha2}}{\partial r}\Big|_{r=b}=J_s; \tag{48}$$

2. The preservation of the magnetic induction components which are normal to the surface of separation between the two media by means of the axial component A_z of the magnetic vector potential (49):

$$B_{n1}=B_{n2}=B_{r1}=B_{r2}\Leftrightarrow$$
$$\Leftrightarrow\frac{\partial A_{\alpha1}}{\partial z}\Big|_{r=b}=\frac{\partial A_{\alpha2}}{\partial z}\Big|_{r=b} \tag{49}$$

Applying the relations (48) and (49) and considering the singularities of the Bessel functions, one can determine the integration constants. P_λ, R_λ, S_λ and T_λ.

For the purpose of calculating the inductances we found appropriate the application of the following relations (50):

$$L_{AA}=\frac{1}{i}\iint_{S_\Gamma}\vec{B}\,\vec{dS}=\frac{1}{i}\iint_{S_\Gamma}rot\vec{A}\,\vec{dS}=\frac{1}{i}\int_\Gamma\vec{A}\,\vec{ds}=\ldots$$
$$\ldots=\frac{1}{i}\int_{C(a-r_c)}A_{\alpha2}(a-r_c,0)\,a\,d\alpha;$$
$$ds=a\,d\alpha; \tag{50}$$
$$L_{AB}=\frac{1}{i}\int_{C(b)}A_{\alpha2}(b,L)\,a\,d\alpha$$

To calculate the inductance L_{AA} (see Figure 4) we've considered a circular curve Γ radius $a - r_c$, marked as $C(a\text{-}r_c)$ where r_c is the radius of turn *A*. For the inductance L_{AB} the curve is the circle *C(b)*.

In the case of several turns, the superposition principle becomes directly applicable, resulting analytic relations expressed by Bessel functions. These inductances can be also calculated with FEM.

The conductance *G* of the insulating material depends on pulsation ω, capacity *C* and the dielectric loss factor $tan\delta$; according to [24], it is calculated with the relation:

$$G=\omega C\,tg\,\delta=2\pi f\,C\,tg\,\delta. \tag{51}$$

3. Assembling the Transformer Winding Model for Overvoltage Stress Study

The transitory regime encountered for overvoltage conditions requires an analysis when using the RLC Ladder Network model. The electrical network built-up requires the division in identical disk coils. Here, the authors have considered a cylindrical winding, divided in 12 disk coils with concentrated parameters (Figure 5), [24,25]. The simulations appeal directly to the schematic circuit from Figure 5 and the results consist of the time variations of the voltages across the disk coils, allowing physical interpretations and evaluations.

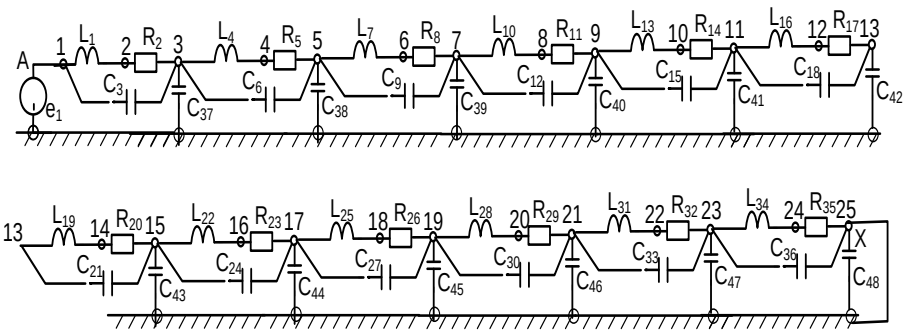

Figure 5. RLC Ladder Network for Overvoltage Study when the Neutral Point is either Insulated (Open Breaker) or Connected to the Ground (Closed Breaker)

3.1. Simulations Regarding the Voltage Distribution across the Transformer Winding

When using the RLC network from Figure 5, there are two versions: one with a homogeneous winding in which the electrical parameters are the same for all disk coils and one non-homogeneous version.

For the latter, the coils from the beginning of the winding have reinforced insulation which results in an augmented space between the turns and decreased values for capacitances. For homogeneous winding case, the electric parameters have the following values, given by (52)-(56).

The values have been calculated from the geometrical dimensions of the transformer having the following data:

$$S_n = 620\ KVA; U_{HV} = 10.5/10/9.5\ kV; U_{LV} = 0.4\ kV.$$

$$L_1 = L_4 = L_7 = L_{10} = L_{13} = L_{16} = L_{19} = L_{22} \cdots \\ \cdots = L_{25} = L_{28} = L_{31} = L_{34} = 4 \cdot 10^{-6}\ H \quad (52)$$

$$R_2 = R_5 = R_8 = R_{11} = R_{14} = R_{17} = R_{20} \cdots \\ \cdots = R_{23} = R_{26} = R_{29} = R_{32} = R_{35} = 2 \cdot 10^{-3}\ \Omega \quad (53)$$

$$C_3 = C_6 = C_9 = C_{12} = C_{15} = C_{18} = C_{21} \cdots \\ \cdots = C_{24} = C_{27} = C_{30} = C_{33} = C_{36} = 30\,pF \quad (54)$$

$$C_{37} = C_{38} = C_{39} = C_{40} = C_{41} = C_{42} = C_{43} \cdots \\ \cdots = C_{44} = C_{45} = C_{46} = C_{47} = C48 = 90\,pF \quad (55)$$

For the non-homogeneous winding case, the only modified values for capacitances C_3, C_6, C_9 are:

$$C_3 = C_6 = C_9 = 7\ pF. \quad (56)$$

The other parameters of the RLC Ladder network (Figure 5) have the same values as in (52)-(56).

3.2. The Description of the Solving Method for the Circuit Equations

The solving method is applicable to a broad class of analog circuits linear and/or nonlinear. These circuits can contain linear and/or nonlinear resistors which can be voltage or current controlled, voltage controlled linear and/or nonlinear capacitors, linear (magnetically coupled or not) and/or nonlinear inductors, current controlled, ideal independent voltage/current sources all types of bi-port sources and generally every single multiport type of element.

The latter includes those multiport elements with an equivalent circuit composed from bipolar elements of circuit and controlled sources only.

The method consists of several steps, with the purpose of performing dynamic (transient) analysis for linear and nonlinear electric circuits. The main steps are:

1. Numerical identification of the elements of the first and second category being in excess and make distinction between their types.

2. Generation of the vector containing the state variables of the circuit under analysis.

3. Calculation of the eigenvalues and eigenvectors. If the circuit is nonlinear and its characteristics are linearized for intervals, the algorithm provides the eigenvalues and eigenvectors for each operating point inside of such interval.

4. Determination of the pulsations of free oscillations of the circuit and their asscociated time constants. From the values of the time constants results the optimal integration steps and the total time of the integation process (final time).

5. Generation of the circuit functions for both types of circuit:SISO (single input, single output) or MIMO (multiple input, multiple output).

The method of equations solely analyses the quality of a circuit and for linear circuits, generates the state equations in Laplace (operational) form.

3.3. Results Obtained Following the Use of SYSEG Program

The main objective of the simulations was the evaluation of time voltage variation for u_{C3}, u_{C6}, u_{C9} and u_{C36} (the voltages across the first three disk coils or capacitances respectively across the last one from the RLC model of Figure 5; these are the voltages across the capacitances C_3, C_6, C_9 and C_{36}) for both cases: homogeneous and non-homogeneous transformer winding under over-voltage stress.

The commutation overvoltage is of sinusoidal type, different from zero for 5 cycles (57):

$$e_1 = \begin{cases} 10 \sin \omega t\ ;\ t \in [0, \dfrac{10\pi}{\omega}] \\ 0\ ;\ t > \dfrac{10\pi}{\omega} \end{cases} \quad (57)$$

Pulsation has two values: one value ω_1 closed to the pulsation of free oscillations ω_0 and another one, ω_2 having a way lower value than ω_0. Due to the fact that $\omega_0 \approx 10^8$ rad/s, the pulsations are: $\omega_1 \approx 10^7$ rad/s and $\omega_2 \approx 2.10^6$ rad/s.

3.3.1. Homogeneous Winding

For such a winding, all of the disk coils have the same electric parameters.

Considering the shape of the overvoltage e_1 (57), the time domain of the variation has two remarkable in sub-intervals: $[0, t_{01}]$ and $[t_{01}, \infty)$. For the first interval the initial conditions are null, while for the second not; the following remarks are valid for the pulsation ω_1:

- $\omega_1 = 10^7$ rad/s $\Rightarrow t_{01} = 31{,}4 \cdot 10^{-7}$s, $e_i = 10.\sin(\omega_1 t)$ *V* and the initial conditions are null;
- $e_i = 0$ and initial conditions different from zero; $\boldsymbol{x}_2(0) = \boldsymbol{x}_1(31{,}4 \cdot 10^{-7})$; $\boldsymbol{x}_1$ – state vector from point 1) and $\boldsymbol{x}_2$ – state vector from point 2)

Similarly, for the pulsation ω_2:

- $\omega_2 = 10^6$ rad/s $\Rightarrow t_{02} = 31{,}4 \cdot 10^{-6}$ s, $e_i = 10.\sin(\omega_2 t)$ *V* and the initial conditions are null;
- $e_i = 0$ and the initial conditions different from zero; $\boldsymbol{x}_2(0) = \boldsymbol{x}_1(31{,}4 \cdot 10^{-6})$; $\boldsymbol{x}_1$ – state vector from point 1) and $\boldsymbol{x}_2$ – state vector from point 2)

The output for the simulation results are the voltages across the capacitances C_3, C_6, C_9 and C_{36}, so the voltages across the first three disk coils and the last one from the RLC model (Figure 5). The first batch of simulations are performed with respect to the pulsation of lower value $\omega_2 = 10^6$ rad/s.

Case A. Simulations for pulsation $\omega_2 = 10^6$ rad/s.

When considering the pulsation $\omega_2 = 10^6$ *rad/s* (which has a much lower value than the pulsation of free oscillations ω_0), the time voltage variation u_{C3} for isolated neutral appears (Figure 6.a) separately from the grounded neutral case (Figure 6.b). This voltage was found across the first coil (Figure 5) through simulations. When considering the isolated neutral, during the interval fulfilling the condition $e_i \neq 0$, the u_{C3} voltage amplitudes are significantly smaller (almost half) than for the situation in which the neutral is grounded.

Conversely, for $e_i = 0$, u_{C3} displays higher values for the winding with isolated neutral in comparison to the situation in which the neutral is grounded. This is explained by the fact that when the neutral is grounded, the variation of u_{C3} voltage depends exclusively upon the overvoltage e_i; when the neutral is isolated, there is an occurrence of overvoltage waveforms across the transformer's winding at the node 25 (Figure 5), due to the fact that node 25 determines a separation between zones of the circuits with much different values for the electrical parameters.

When considering the frequency (pulsation) domain, no major interaction between the pulsation of overvoltage e_1 and free oscillations pulsation ω_0 can be accounted for. In fact, the pulsation of the free oscillations ω_0 has a much larger value than ω_2, which makes the time variation of the voltage u_{C3} to be determined mainly by the overvoltage e_1 and the reflection of the overvoltage waveforms in the nodes which separate circuit zones having different values of electrical parameters. For the purpose of following the overvoltage distribution across the disk coils, Figure 7 displays the voltage across the second disk coil u_{C6}.

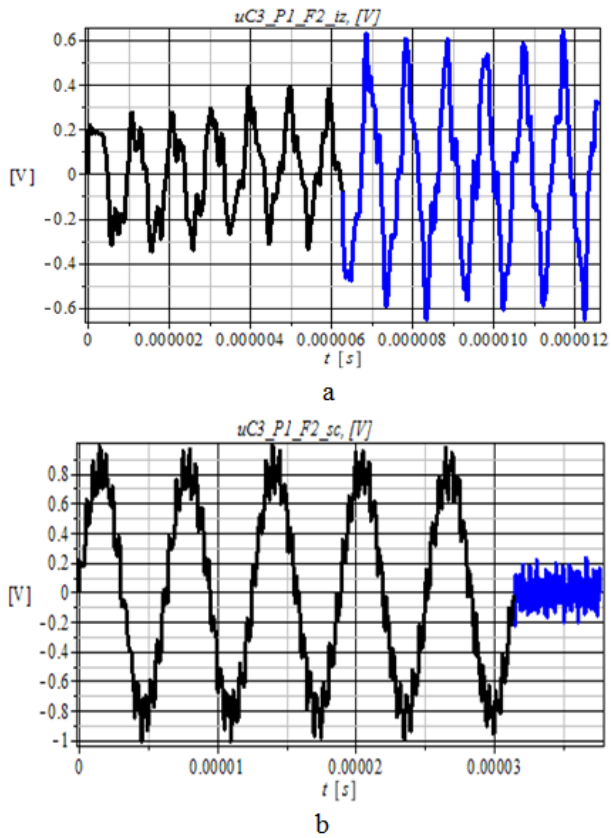

Figure 6. Time variation of the voltage u_{C3} for $\omega_2 = 10^6$ *rad/s*: a) winding with isolated neutral; b) winding with grounded neutral

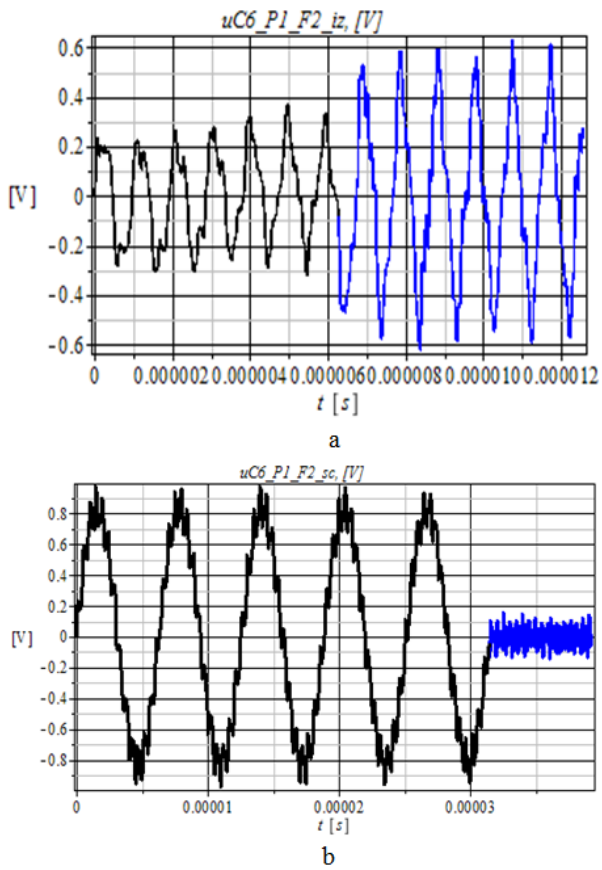

Figure 7. Time variation of the voltage u_{C6} for $\omega_2 = 10^6$ *rad/s*: a) winding with isolated neutral; b) winding with grounded neutral

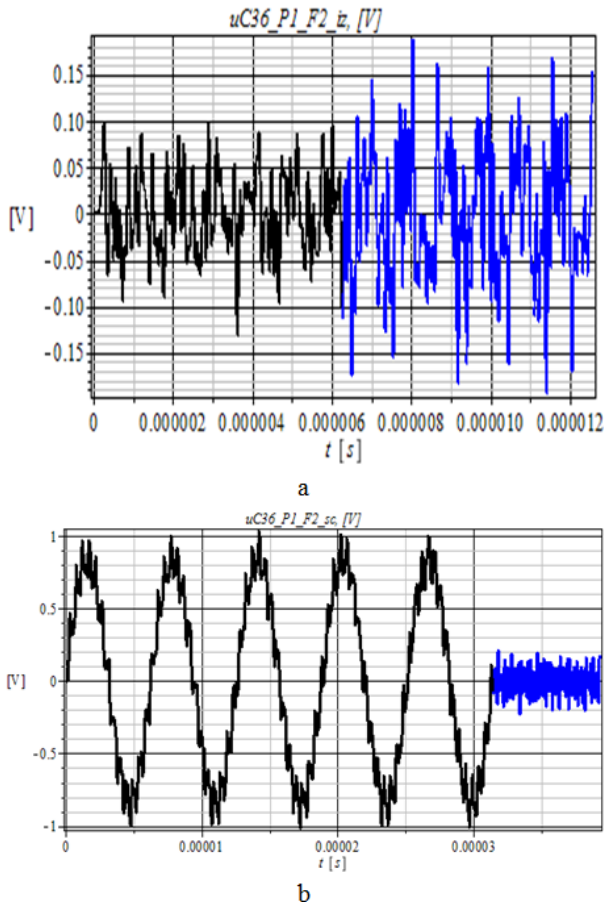

Figure 8. Time variation of the voltage u_{C36} for $\omega_2 = 10^6$ *rad/s*: a) winding with isolated neutral; b) winding with grounded neutral

Both overvoltages u_{C3} and u_{C6} display similar shapes of the waveforms representing their time variations. However, the voltage across the second disk coil u_{C6} has slightly lower amplitudes with respect to u_{C3}, more evidently when $e_i = 0$, yet with no notable differences. The time variation of the voltage u_{C36} (Figure 8) is significantly different from u_{C3} and u_{C6}, especially when the winding has the neutral isolated. In this case there the overvoltage distribution is profoundly non-uniform.

The voltage across the last coil has way lower amplitude values with respect to the voltages u_{C3} and u_{C6} for both intervals ($e_i \neq 0$ and $e_i = 0$). For the winding with grounded neutral there are very little variations for the voltages u_{C3}, u_{C6} şi u_{C36}. The overvoltage distribution is almost uniform in this case.

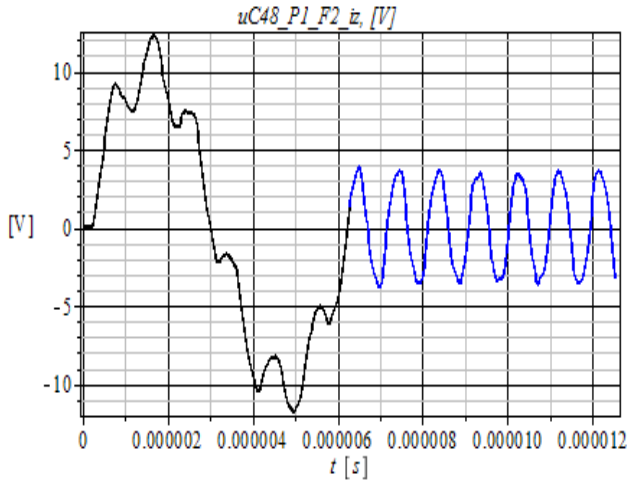

Figure 9. Time variation of the voltage u_{C48} for $\omega_2 = 10^6$ *rad/s* and winding with isolated neutral

The observations and conclusions cover a 12 µs interval; after a longer duration, all the voltages across the disk coils will approach zero value. The main difference between the two cases is represented by the node 25. The voltage u_{C48} across the capacitor C_{48} offers a good explanation (Figure 9) for the differences encounterd in both situations regarding the neutral point of the winding. When the neutral point is isolated, due to the multiple reflections occured at the node 25, most of the overvoltage is recorded at the terminals of the capacitor C_{48}.

Case B. Simulations for the pulsation $\omega_1 = 10^7$ rad/s.

This pulsation, having much closer value to the free oscillation pulsation than ω_2, is the originator of much higher voltages across the disk coils that in study case A. All of the phenomena analyzed in case "A" are still present, yet insignificant in comparison with the resonance phenomena occurring between the pulsation of the overvoltage e_1 and the free oscillations.

For case B, the recorded overvoltages u_{C3} and u_{C6} across the disk coils have much higher amplitudes than in case A (see Figure 10 and Figure 11).

The overvoltage applied across the last turns of the transformer winding records dangerously high values in this case.

The voltages across the disk coils display a slight decay once the distance with respect to the terminal A increases. The last coil from the *RLC* model (Figure 5) withstands the highest voltage stress when the neutral point is connected to the ground (Figure 12).

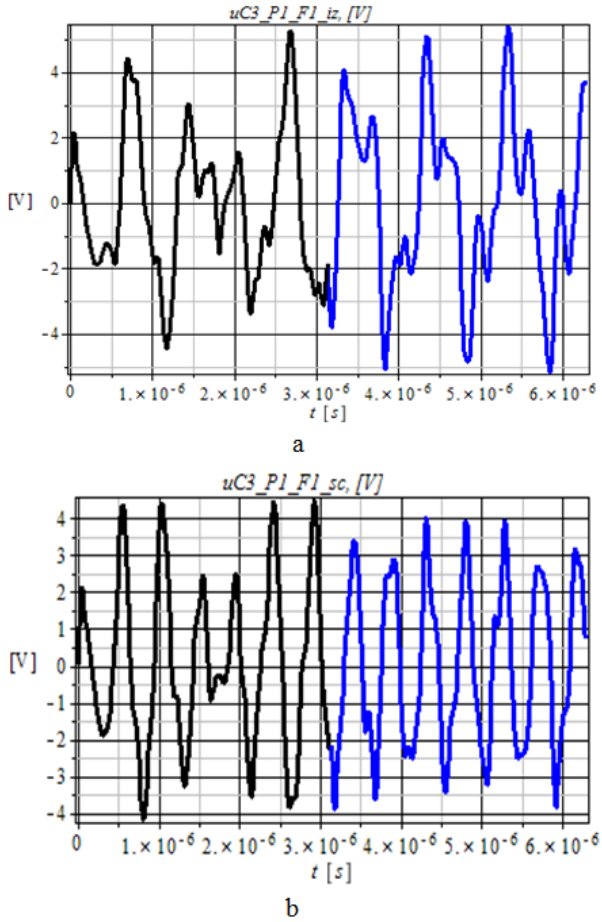

Figure 10. Time variation of the voltage u_{C3} for $\omega_1 = 10^7$ *rad/s*: a) winding with isolated neutral; b) winding with grounded neutral

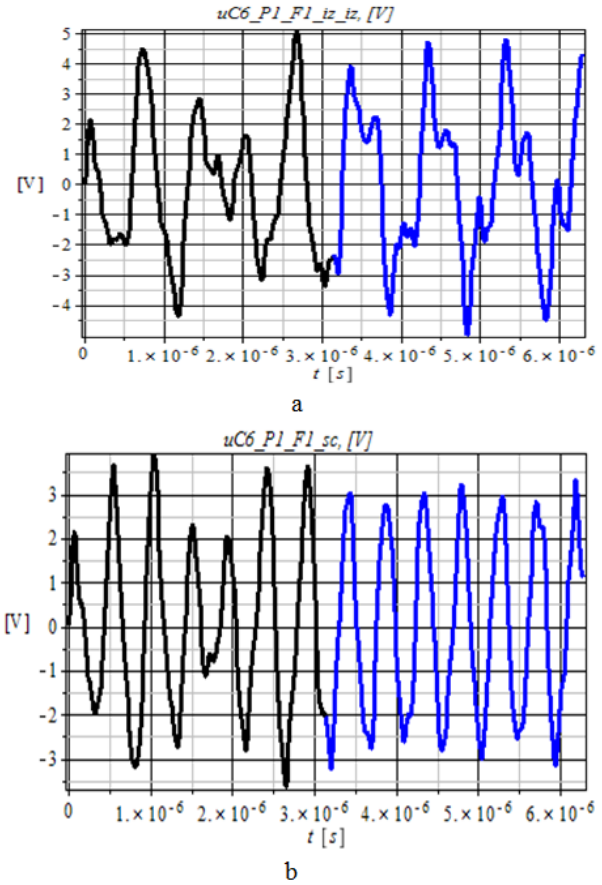

Figure 11. Time variation of the voltage u_{C6} for $\omega_1 = 10^7$ *rad/s*: a) winding with isolated neutral; b) winding with grounded neutral

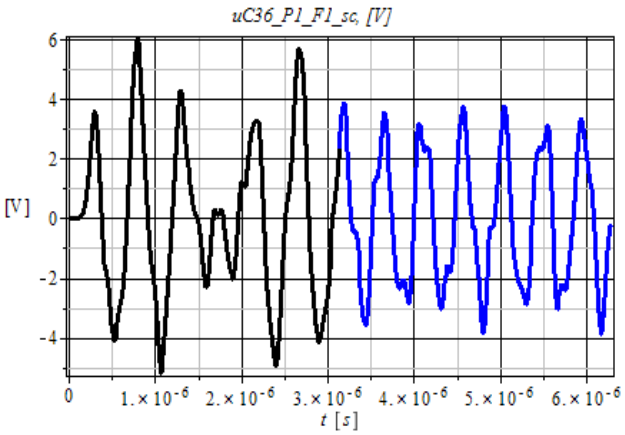

Figure 12. Time variation of the voltage u_{C48} for $\omega_1 = 10^7$ *rad/s* and winding with grounded neutral

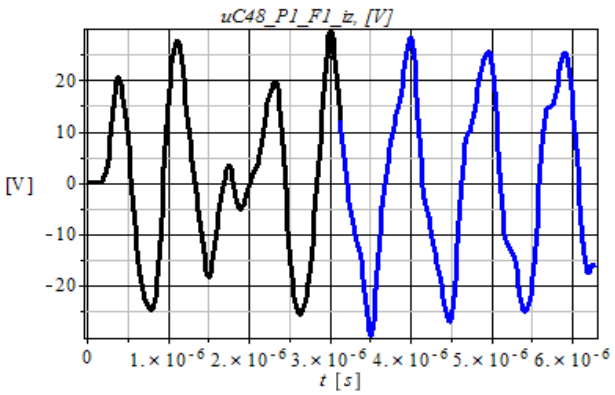

Figure 13. Time variation of the voltage u_{C48} for $\omega_1 = 10^7$ *rad/s* and winding with isolated neutral

When the winding has the neutral isolated, u_{C48} displays the highest amplitude values (Figure 13); the last few turns of the winding have to withstand a very high voltage amplitude. The difference in amplitudes of the voltages between the case of the winding with grounded neutral and the case of the winding with the isolated neutral has the same reason as in case A.

Case C. Simulation for step overvoltage e_1 = 10 V.

For step up overvoltage, the voltage across the transformer winding has a very fast transient. This results in very high values of the voltages across the disk coils (see Figure 12 for the case of the winding with neutral isolated, respectively Figure 13 for the case of the winding with grounded neutral).

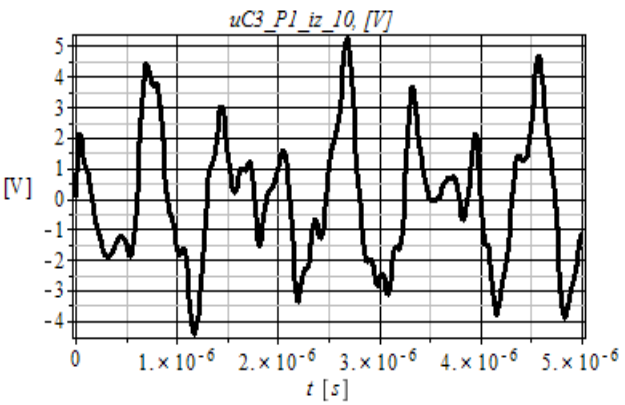

Figure 14. Time variation of the voltage u_{C3} for step over-voltage and winding with isolated neutral

Similar explanations with the previous cases are valid. When encountering a step type of variation, the overvoltage e1 varies as fast as in the situation of free oscillations.

When analyzing the simulation results, the non-uniformity of the voltage distribution across the winding appears enhanced in the case of the winding has neutral isolated than for the winding with the neutral connected to the ground.

The voltage u_{C48} encounters very high amplitude (see Figure 16).

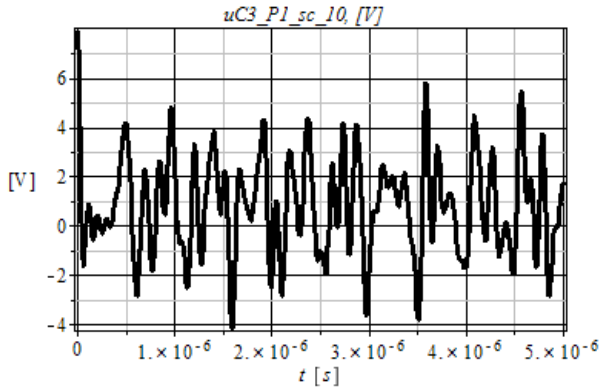

Figure 15. Time variation of the voltage u_{C3} for step over-voltage and winding with grounded neutral

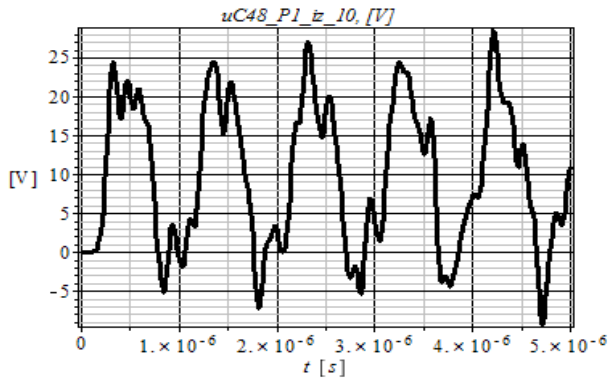

Figure 16. Time variation of the voltage u_{C48} for step overvoltage and winding with isolated neutral

3.3.1. Non-Homogeneous Winding

Usually, the first turns from the beginning of the winding have reinforced insulation to withstand overvoltage transients, knowing that the voltage distribution is non-uniform across the winding.

In this case, the inter-turn capacitances for the first turns have lower values than the capacitances of the inter-turns in continuation [9]. In simulations, the authors considered the capacitances defined by the relationships (55), (56).The non-homogeneous character of the winding is enhanced, considering the values given by (56). There are some modifications explained by the overvoltage waveform reflections occurring at node 7 during propagation. For example, from the simulations, Figure 15 displays the time variation of the voltage $u_{C3.}$

When considering the winding with the isolated neutral, the time variation of the over-voltage is significantly different with respect to homogeneous winding situation; when considering the first disk coils, the voltages u_{C3}, u_{C6} şi u_{C9} have almost the same value for their lower

amplitudes being affected more by the reflections encountered at the node 7.

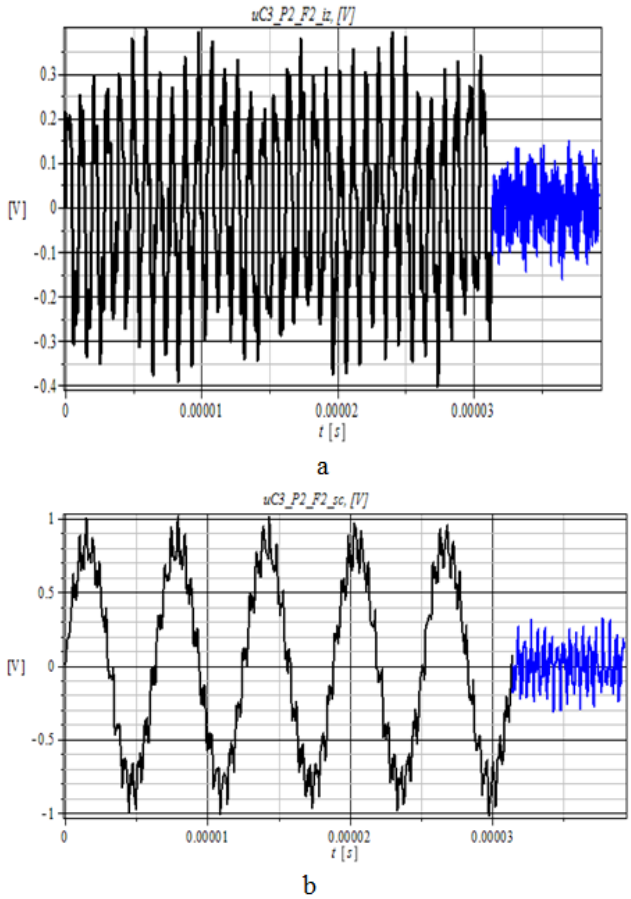

Figure 17. Time variation of the voltage u_{C3} for $\omega_2 = 10^6$ *rad/s*: a) non-homogeneous winding with isolated neutral; b) non-homogeneous winding with grounded neutral

For the winding with grounded neutral, there are no significant modifications

Similarly to the homogeneous winding situation, the non-uniformity of the overvoltage distribution across the winding is more evident when the winding has an isolated neutral. For highly non-uniform windings, which can display much larger electrical parameter variations, the differences in terms of the over-voltage distribution can be more important.

4. Conclusions

We have analyzed the transformer winding model in two situations: first, with distributed electrical parameters, and secondly with concentrated electrical parameters.

The development of the mathematical model of the winding with distributed parameters included the general case of model for the long lines as well as the model used for the distribution of the overvoltage across the winding. The *RLC model* was adapted to be suitable for the overvoltage study across the transformer winding. Phenomena related to both types of overvoltages (commutation and step type) have been assessed when using the program SYSEG in simulations.

The information extracted from the time variation of the voltages across the disk coils appears more consistent when focusing on the times of peak voltage; however, when representing the voltage distribution for randomly chosen times, it appeared unlikely to capture exactly the moments of maximal voltage amplitude.

When considering the commutation overvoltages, the amplitudes reach maximum values at different instants and not obviously of the waveform.

The study considered two values of the commutation overvoltage pulsation: one pulsation ω_1 having a close value to the characteristic pulsation free oscillations ω_0, and a pulsation ω_2 which is much less than ω_0. With the use of SYSEG program, information voltage distribution across the winding became available for both types of windings: homogeneous and non-homogeneous.

In both cases the voltage distribution was almost uniform. Meanwhile, the overvoltage pulsation had a much lower value than the free oscillations pulsation. The uniform distribution becomes even more evident if the pulsation approaches the value of the free oscillations pulsation.

This uniform distribution is explained by the fact that for pulsation values approaching resonance, the oscillation voltage amplitude increases significantly. If the overvoltage pulsation would be able to exceed the value of the free oscillation pulsation, then the non-uniformity of the overvoltage distribution across the winding would increase with the increasing of the overvoltage pulsation. Time variation of the overvoltage would become very fast despite the fact that would not be in the resonance zone. The voltages across the coils sometimes display higher values when the neutral is grounded. This is due to the fact that, when the neutral is grounded there is a larger gap between the electrical parameters values.

For the winding with an isolated neutral, a significantly large fraction of the overvoltage was recorded across the terminals of the last capacitance (see Figure 5 for the RLC model) and the last turns of the winding were highly stressed. Similar phenomena were related to the non-homogeneous windings. However, the time variation of the overvoltage waveform was significantly different and the first disk coils encountered an even electrical stress. The winding can be assembled from several sections with electrical parameters having different values.

References

[1] Y. Shibuya, S. Fujita, and N. Hosokawa, (1997) "Analysis of very fast transient over voltage in transformer winding," *Proc. Inst. Elect. Eng., Gen. Trans. Distrib.*, vol. 144, no. 5, pp. 461-468.

[2] S. M. Hassan Hosseini, Mehdi Vakilian, and Gevork B.; Gharehpetian, (2008) "Comparison of Transformer Detailed Models for Fast and Very Fast Transient Studies," *IEEE Trans. on Power Delivery*, vol. 23, no. 2, pp. 733-741.

[3] M. Popov, L. V. Sluis, and G. C. Paap, (2003) "Computation of very fast transient over voltages in transformer windings, " *IEEE Trans. Power Del.*, vol. 18, no. 4, pp. 1268-1274.

[4] M. Popov, L. van der Sluis, R. P. P. Smeets, and J. Lopez Roldan, (2007) "Analysis of very fast transients in layer-type transformer windings," *IEEE Trans. Power Del.*, vol. 22, no. 1, pp. 238-247.

[5] J. L. Guardado and K. J. Cornick, (1989) "A computer model for calculating steep-fronted surge distribution in machine windings," *IEEE Trans. Energy Convers.*, vol. 4, no. 1, pp. 95-101.

[6] P. G. McLaren and H. Oraee, (1985) "Multiconductor transmission-line model for the line-end coil of large AC machines," *Proc. Inst. Elect. Eng. B*, vol. 132, no. 3, pp. 149-156.

[7] Z. Azzouz, A. Foggia, L. Pierrat, and G. Meunier, (1993) "3D finite element computation of the high frequency parameters of

power transformer windings", *IEEE Trans. Magn.*, vol. 29, no. 2, pp. 1407-1410.

[8] D. J. Wilcox, M. Conlon, and W. G. Hurley, (1988) "Calculation of self and mutual impedances for coils on ferromagnetic cores," *Proc. Inst. Elect. Eng.*, vol. 135, no. 7, pp. 470-476.

[9] Guishu Liang, Haifeng Sun, Xile Zang and Xiang Cui (2006) "Modeling of Transformer Windings under Very Fast Transient Overvoltages," *IEEE Transactions on Power Delivery*, vol. 48, no. 4, pp. 733-741.

[10] R. M. Del Vecchio, B. Poulin, and R. Ahuja, (1998) "Calculation and measurement of winding disk capacitances with wound-in-shields," *IEEE Trans. Power Del.*, vol. 13, no. 2, pp. 503-509.

[11] M. Eslamian and B. Vahidi (2012) "New Methods for Computation of the Inductance Matrix of Transformer Windings for Very Fast Transient Studies," *IEEE Trans. Power Del.*, vol. 27, no. 4, pp. 2326-2333.

[12] A.Ahmad and Ph. Auriol (1992) "Conformal Mapping Method for Calculation of Rectangular Winding Parameters," *IEEE Trans. Magn.*, vol. 28, no. 5, pp. 2823-2825.

[13] K.G.N.B Abeywickrama, A.D. Podoltsev, Y.V. Serdyuk, S.M. Gubanski (2007) "Computation of Parameters of Power Transformer Windings for Use in Frequency Response Analysis," *IEEE Trans. Magn.*, vol. 43, no. 5, pp. 1983-1990.

[14] A.D. Podoltsev, K.G.N.B Abeywickrama, Y.V. Serdyuk, S.M. Gubanski (2007) "Multiscale Computations of Parameters of Power Transformer Windings at High Frequencies. Part II: Large Scale Level," *IEEE Trans. Magn.*, vol. 43, no. 12, pp. 4076-4082.

[15] P. Gomez, and F. de Leon, (2011) "Accurate and Efficient Computation of the Inductance of Transformer Windings for the Simulation of Very Fast Transients," *IEEE Trans. Power Del.*, vol. 26, no. 3, pp. 1423-1431.

[16] A. Boyajian, (1954) "Leakage Reactance of Irregular Distributions of Transformer Windings by the Method of Two Fourier Series," *AIEE Trans. Power App. Syst.*, vol. 29, no. 2, pt. 3, pp. 1407-1410.

[17] L. Rabins, (1956) "Transformer Reactance Calculations with Digital Computers," *AIEE Trans.* vol. 75, pt. 1, pp. 261-267.

[18] A. Predota and Zdenka Benesova, (2011) "Fast Transeinet Overvoltage in Transformer Winding," *Przeglad Elektrotechniczny (Electrical Review)*, ISSN 0033-2107, R. 87, NR. 5, pp.142-145.

[19] K. Prakasam, M. Surya Kalavathi, D. Prabhavathi (2016) "Analysis of Very Fast Transient Over Voltages (VFTOs) of Transformer in Gas Insulated Substations (GIS) using Wavelet Techniques," *Proc. of 3rd International Conference on Electrical, Electronics, Engineering Trends, Communication, Optimization and Sciences (EEECOS) -2016*, pp. 749-755.

[20] Tao Wang, Huaying Dong and Guishu Liang (2008) "Overvoltage Distribution Calculation of Transformer Windings under VFTO Considering Frequency-dependent Parameters via Krylov Subspace Technique," *Proc. of 3rd International Conference on Electric Utility and Restructuring and Power Technologies , DRPT2008* , Nanjing, China, 6-8 April 2005, pp. 887-889.

[21] M. Bagheri, M. Vakilian, A. Hekmati and R. Heidarzadeh (2007) "Influence of Electrostatic Shielding of Disc Winding on Increasing the Series Capacitance in Transformer," *Power Tech 2007*, Laussane, Switzerland, July 1-5, pp.1780-1784.

[22] M. Heidarzadeh and M.R. Besmi (2013) "Influence of Transformer Layer Winding Parameters on the Capacitive Characteristic Coefficient," *International Journal on Technical and Physical Problems of Engineering*, (IJTPE) ISSN 2077-3528, Issue 15, Vol. 5, No. 2, pp. 22-28.

[23] M. Heidarzadeh and M.R. Besmi (2014) "Influence of the Parameters of Disk Winding on the Impulse Voltage Distribution in Power Transformers," *Iranian Journal of Electrical and Electronic Engineering*, Vol.10, No.2, pp.143-141.

[24] S.G. Bontidean, F. Rezmerita, M.Iordache, N. Galan, (2013)Analiza prin simulare a distribuției supratensiunilor în înfășurarile transformatorului; SME 2013, București (in Romanian).

[25] M. Iordache, S. Deleanu, Gloria Ciumbulea, Lavinia IORDACHE (BOBARU), N. Galan, (2014) "Distribuția supratensiunii de comutație in lungul înfășurării transformatorului electric," SME 2014, București (in Romanian).

[26] M. Iordache, Lucia Dumitriu, D. Delion (2000) "**S**YSEG – SYmbolic State Equation Generation", User's Manual, Catedra de Electrotehnică, U.P.B., București (in Romanian).

[27] M. Iordache, Lucia Dumitriu**,** (2000**) "**Symbolic state equations for analog circuits", Revue Roum. Sci. Techn.- Électrotechn. et Énerg., Bucarest , tom 45, nr.1, pp. 21-37.

[28] M. Iordache, Lucia Dumitriu, I. Matei, (2002) "SYMNAP – SYmbolic Modified Nodal Analysis Program", User Guide, Electrical Department Library, Politehnica University of Bucharest.

[29] N. Galan (2011) Maşini electrice, Editura Academiei Române, București.